RSC Advances

ROYAL SOCIETY OF CHEMISTRY

www.rsc.org/advances

Surface imprinting of g-C_3N_4 photocatalyst for enhanced photocatalytic activity and selectivity on photodegradation of 2-Mercaptobenzothiazole

Zhi Zhu[a], Ziyang Lu [b], Xiaoxu Zhao [a], Yongsheng Yan[a*], Weidong Shi [a*], DandanWang [a], Lili Yang [a], Xue Lin [a] , Zhoufa Hua [a], Yang Liu [a]

a School of Chemistry and Chemical Engineering, Jiangsu University, China

b School of the Environment and Safety Engineering, Jiangsu University, China

*Corresponding author Tel.: +86 511 8879 0187 Fax. : +86 511 8879 1800
E-mail address: gchxz206@126.com

ABSTRACT:

In the present work, based on Fe_3O_4/g-C_3N_4 as the support, 2-mercaptobenzothiazole (MBT) as the template molecule, pyrrole as functional monomer, we synthesized the significantly efficient, stable, magnetic conductive imprinted photocatalysts (MCIPs) through suspension polymerization method. Moreover, the MCIPs not only exhibited higher photodegradation capacity to MBT under visible light irradiation, but also possessed good selectivity. The specific surface areas of the resultant MCIPs were approximately four times to that of pure g-C_3N_4. Furthermore, the result indicated that h^+ was the major reactive species in the photocatalytic reaction system. The photodegradation mechanism was also discussed through analyzing the mass spectrum (MS), and the result demonstrated that MBT was degraded to H_2O, CO_2 and other small molecules step by step. In addition, after five cycles, MCIPs still showed higher photocatalytic efficiency, indicating that the as-prepared MCIPs had excellent photochemical stability and a better application prospect in water treatment.

Keywords: selectivity, conductivity, magnetic, molecularly imprinted polymers, g-C_3N_4, 2-Mercaptobenzothiazole

INTRODUCTION

In recent years, much attention has been paid to the environmental problems, a number of organic pollutants in contaminated water, such as the high toxic, persistent and malodorous [1-2]. Especially the contaminants of mercaptan, which was common in waste water, emitting a strong foul odor and threating the health of people [3]. Inhalation of low concentrations of MBT (a kind of mercaptan) vapor can cause headache, nausea; High concentrations can cause fatal respiratory paralysis, this serious problem indicate that selective removal [4-6] MBT from waste water is necessary and important. Therefore, many traditional methods to remove the pollutants from the aquatic environment had been used, such as filtering method, adsorption and microbial degradation. Unfortunately, all of these ways cannot remove the pollutants completely. Nowadays, photocatalytic technology received significant attention, due to its attractive applications in environmental cleaning and energy conversion. Nevertheless, the common properties of photocatalytic technology and photocatalysts materials can not be identified and selective degradation of special molecules.

In order to solve the problem above, many photocatalytic materials have attracted particular attention to remove of organic pollutants in waste water [7], Currently, g-C_3N_4 as one of the most promising photocatalysts has been concerned by many researchers [8-9], the high

stability in aqueous solutions, easy preparation and visible light responsive semiconductor with a moderate band gap (Eg =2.7eV) [10-14]. Unfortunately, the pure g-C_3N_4 as visible-light photocatalys has three main drawbacks. 1) Difficult to collection of the sephotocatalysts [15]. 2) The poor selectivity of g-C_3N_4 to remove the target molecule from complicated pollutants. 3) Lower visible-light photocatalytic efficiency. Thus far, a simple way to simultaneously address these issues has yet to be achieved.

In order to overcome above basic disadvantages of g-C_3N_4, 1) Fe_3O_4 nanoparticles as the magnetic materials loaded on g-C_3N_4 nanosheets, on the one hand, due to its good magnetic properties for improving the recycle efficiency [16], On other hand, the excellent conductive as high as 1.9×10^6 Sm^{-1} [17, 18], which transfer electron-holes pairs rapidly. 2) for enhanced the selectivity of g-C_3N_4, surface imprinting technology is used [19], which is the most attractive and widely used method for preparing imprinted polymer with the ability of recognizing the target molecule. Therefore, surface imprinting technology can modify the surface of g-C_3N_4 and improve the ability of selective recognition MBT , then achieve the goal of photodegradation MBT. 3) While using imprinting technique and modifying g-C_3N_4 by special polymers [20] will improve the selectivity and also reduce the catalytic activity, active site will be covered, therefore, requires the formation of imprinting layer have

special requirements. The imprinting layer should synergy to catalyst, enhanced the catalytic activity and selectivity. That is why polymeris more important for synthesis imprinted layer. In particular, PPy showed great optical properties, unique electrical, excellent stability, and photocatalysis [21-23]. Furthermore, PPy is also an efficient holes transporter and better electron donor with visible light excitation, which proposed that polypyrrole has the ability to oxidize the pollutants. Some works have been carried out to investigate the photocatalytic activity of PPy-modified TiO_2, PPy/Bi_2WO_6 composite and found that the modification of PPy can effectively enhance the photoactivity [24–26].

According to our knowledge, no method was proposed to enhance the selectivity and catalytic activity for g-C_3N_4 on degradation of MBT until now. Therefore, our group using the surface imprinting technology, which is the high polymer preparation with specific recognition of target molecular technology, applied an easy method to synthesize MCIPs for selective degradation of MBT. In present work, the MCIPs were successfully prepared based on Fe_3O_4/g-C_3N_4 as the support, MBT as the template molecule, pyrrole as functional monomer. And further characterized by X-ray diffraction (XRD), fourier-transformed infrared spectra (FT-IR), transmission electron microscopy (TEM), high-resolution TEM (HRTEM), scanning electron microscope (SEM), Brunauer–Emmett–Teller (BET) method, thermogravimetric analysis

(TGA), elemental analysis, vibrating sample magnetometer (VSM), photoluminescence (PL), element analysis. In addition, a series of influencing factors were optimized (such as the amount of functional monomer, the polymerization time). Afterwards, the experiments of adsorption, photocatalytic degradation and selectivity were also investigated. Finally, the mechanism for degradation of MBT over the MCIPs was also discussed.

2. EXPERIMENTAL SECTION

2.1. Materials.

All chemicals were used without further purification, distilled water was used in the whole experiments. Melamine (AR), iron (III) chloride hexahydrate ($FeCl_3 \cdot 6H_2O$, AR), iron (II) chloride tetrahydrate ($FeCl_2 \cdot 4H_2O$, AR), 2-mercaptobenzothiazole (MBT), and trimethylolpropanetrimethacrylate (TRIM, AR) were all supported by Aladdin Chemistry Co., Ltd. Polyethylene glycol 4000 (PEG 4000, CP), trichloromethane (AR), NH_4OH solution (25.0%), pyrrole (CP), p-benzoquinone (BQ, AR), isopropanol (IPA, AR), triethanolamine (OA, AR), ethanol (C_2H_5OH, AR) were all purchased from Sinopharm Chemical Reagent Co., Ltd. Azodiisobutyronitrile (AIBN, CP) was obtained from Shanghai No.4 Reagent & H.V. Chemical Co., Ltd.

2.2. Preparation of g-C_3N_4.

The pure g-C_3N_4 sample was synthesized by heating melamine. Briefly,

10 g melamine was heated from room temperature to 500℃ with the heating rate of 4℃ min^{-1} and kept at 500℃ for 2 h. Afterwards, the product was further heated to 520℃ with the heating rate of 4℃ min^{-1} and kept at 520℃ for another 2 h. After cooling to room temperature, the powder of g-C_3N_4 was obtained and grinded for further use.

2.3. Preparation of Fe_3O_4/g-C_3N_4.

The Fe_3O_4/g-C_3N_4nanocomposites were prepared by Santosh Kumar's method with mild changes [19]. Firstly, g-C_3N_4 (2.2g) was dispersed in 600mL of ethanol/water (1:3) and ultrasound (PCI Analytics, 12 mm probe, 33 Hz, 150 W) for 5 h at ambient temperature. Secondly, $FeCl_3 \cdot 6H_2O$ (2 mmol) and $FeCl_2 \cdot 4H_2O$ (1 mmol) were dissolved separately in 20mL of double-distilled water and added to the suspension of g-C_3N_4 stirring at 80°C for 30 min. Subsequently, 10 ml NH_4OH solution was quickly injected into the reaction mixture, and stirred for another 30 min. Finally, the Fe_3O_4/g-C_3N_4 was washed several times with water and ethanol, then dried in vacuum and collected by magnet.

2.4. Preparation of MCIPs.

1g Fe_3O_4/g-C_3N_4 and 1g PEG were added into three flask containing 100 ml deionized water with stirring 30 min. Meanwhile, 0.3 mmol MBT (template molecule), 0.1 ml TRIM (cross-linker) and 0.3 mmol AIBN (initiator) were dissolved into 15 ml trichloromethane which contained 6mmol pyrrole, sonicated 10 min for dissolved completely. Afterward, the

mixed solution was added into the above solution. The reaction has been stirring for 24 h under protection of nitrogen at 75℃. Finally, after the solid product was washed by soxhlet extraction with methanol and glacial acetic acid and dried by vacuum drier, MCIPs were obtained. No imprinted catalysts (MCNIPs) was prepared by the same procedure for MCIPs only absence of MBT. In order to understand preparative procedure of MCIPs composites easily, the synthesis route and preparation process were described in Scheme. 1

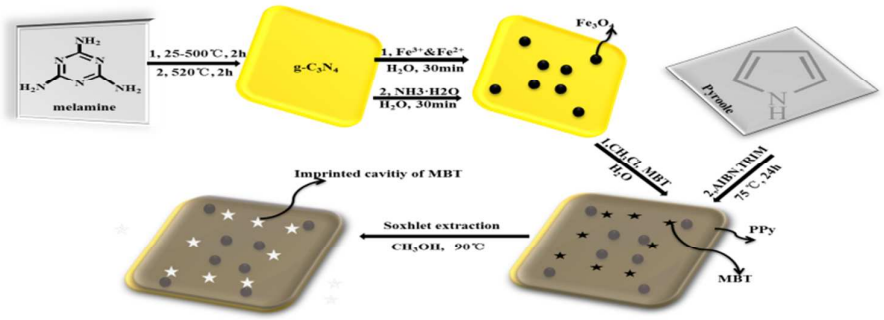

Scheme. 1 Schematic Representation of MCIPs

2.5. Adsorption experiments.

In order to compare the adsorption capability of MCIPs and g-C_3N_4 to MBT, the adsorption capacity was detected as below. 0.1 g photocatalyst was added into catalytic reactor which equipped with 100 ml 10 mg L^{-1} MBT aqueous solutions. 8 ml solution were sampled with an injector in 10 min interval, after stirring for 60 min in the dark at 30℃, the solution was filtered and the concentration of MBT was measured by UV–vis spectrophotometer.

2.6. Photocatalytic activity and selectivity experiments.

In order to study the photocatalytic activity of g-C_3N_4, MCIPs and MCNIPs on degradation of MBT, the reaction should reach adsorption-desorption equilibrium. The adsorption procedure was consisted with section 2.5. After the reaction reached the adsorption-desorption equilibrium, the xenon lamp (300 W) and the aeration were both turned on, maintained the reaction time for 1 h. Next, the absorbance of the sample was measured by Ultraviolet spectrophotometer after magnetic separation. In order to investigate the selectivity, another contaminant (danofloxacin mesylate) was chosen, and the experiment steps were as same as above.

2.7. Circulation experiment.

The reusability of MCIPs was very important from a practical application point of view. Therefore, five groups of successive MBT degradation experiments were produced. First step, the photodegradation experiment was carried out according to section 2.6. Subsequently, the sample was collected with a magnet and washed with ethanol. After drying, the sample was used as the second cycle experiment. Afterwards, the remaining four cycle steps were the same as the first step.

2.8. Characterization.

In order to analyze the performance of catalyst, lots of characterizations had been done as follows: The X-ray diffraction (XRD) were used to characterize the crystal structure, and the patterns of the

photocatalyst were obtained with a D/max-RA X-ray diffractometer (Rigaku, Japan) which equipped with Ni-filtrated Cu Ka radiation (40kV, 200mA) at 5-80° with a scanning step of 0.02°/0.2s. Both the scanning electron microscope (SEM) images and X-ray energy diffraction spectrum (EDS) were performed with JSM-7001F scanning electron microscopy (JEOL Ltd., Japan). The transmission electron microscope (TEM) images were examined with JEM-2100 transmission electron microscopy (JEOL, Japan). Fourier transform infrared spectra (FT-IR) were recorded on a Nicolet Nexus 470 FT-IR (America thermo-electricity Company) with 2.0 cm^{-1} resolution in the range 400cm^{-1}-4000 cm^{-1}, using KBrpellets. Themagnetic was carried out by using a vibrating sample magnetometer (VSM) (HH-15, Jiangsu University). Specific surface areas were obtained by the Brunauer-Emmett-Teller (BET) method and examined with a NOVA 2000e analytical system (Quantachrome Co., USA). Thermogravimetric analysis (TGA) was carried out by thermal analyzer (NETZSCHGeratebau GmbH, Germany) in the air atmosphere up to 800□ from room temperature with a heating rate of 10□ min^{-1}. The elemental content of each sample were analyzed by Elemental analyzer (EA-1112A, Thermos, Italy). The photoluminescence (PL) emission spectra of samples were detected with a fluorescence spectrophotometer (Cary Eclipse Spectrophotometer, VARIAN, USA) using a xenon lamp as the excitation source at room temperature. The degradation mechanism of

tetracycline aqueous solution was detected by the Thermo LXQ mass spectrometry (MS).

3. RESULTS AND DISCUSSION

3.1.1 XRD analysis

Fig. 1 showed the XRD patterns of pure g-C_3N_4, Fe_3O_4/g-$C_3N_4$and MCIPs. Characteristic peaks of g-C_3N_4 was actually seen at 2θ=27.4° and 13.1° corresponding to the PDF #50-1250 date file [27], which was also appeared in Fe_3O_4/g-C_3N_4 and MCIPs, this result indicated that the structure of g-C_3N_4 did not change by adding Fe_3O_4 and PPy, or other materials. Moreover, six distinct typical peaks (2θ=30.2°, 35.5°, 43.2°, 53.4, 57.3° and 62.6°) were observed in Fig. 1b and Fig. 1c, which were attributed to the magnetite of Fe_3O_4 nanoparticle [16]. However, the diffraction peaks of PPy were not detected in Fig. 1c, it's difficult to judge whether MCIPs had been successfully prepared from XRD pattern, but this was proved by the characterization of FT-IR, SEM, TEM and elemental analysis.

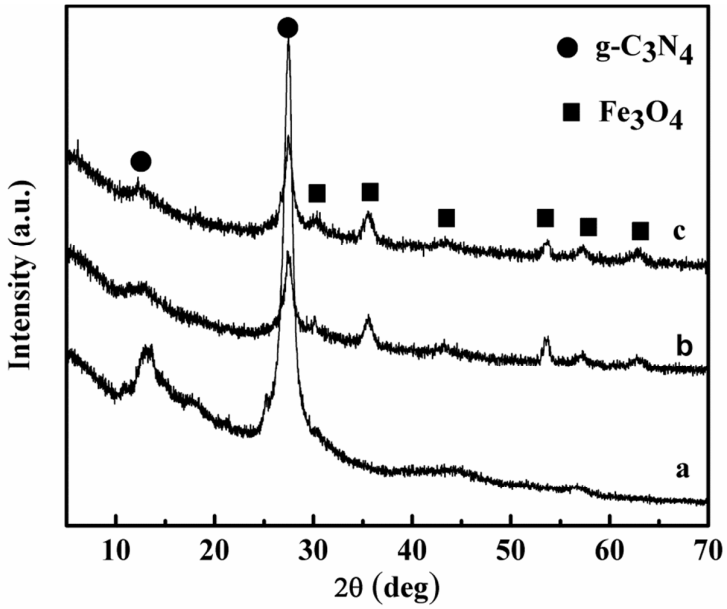

Fig.1 XRD patterns of the samples: g-C_3N_4 (a), Fe_3O_4/g-C_3N_4 (b) and MCIPs (c)

3.1.2 FT-IR

The FT-IR spectra of pureg-C_3N_4, Fe_3O_4/g-C_3N_4 and MCIPs were shown in Fig. 2. A series of peaks at 1650 cm^{-1}-1200 cm^{-1} (1251, 1325, 1419, 1571, and 1639 cm^{-1}) were corresponded to the typical stretching modes of CN heterocycles [28-29], such as C-N and C=N stretching [30, 31]. The peak near 808 cm^{-1} was attributed to the typical bending vibration of s-triazine units [32]. The broad peaks from 3400 cm^{-1} to 2800 cm^{-1} in all three materials were the stretching vibrational modes of primary (=NH) and secondary (-NH) amines [33]. In the spectrum of Fe_3O_4/g-C_3N_4 and MCIPs, the peak at 550 cm^{-1}-650 cm^{-1} was corresponded to the Fe-O [34, 35]. The results showed that Fe_3O_4 has been successfully loaded on the surface of g-C_3N_4. With regard to the MCIPs, as reported in the literature [36], PPy exhibits the characteristic

absorption bands at 1575, 1468, 1298, 784 and 678 cm^{-1}. They were assigned to pyrrole ring stretch, C-H in-plane deformation and C-H outer-bending vibrations, respectively. Some characteristic absorption bands also appeared in the FT-IR spectrum of MCIPs, however, these characteristic bands became stronger (1575 cm^{-1}) or unclearly (784 cm^{-1}, 678 cm^{-1}) in the spectrum, which might due to the overlap of the FT-IR spectra of g-C_3N_4, low concentration of PPy in the composites and the possible interplay of PPy with g-C_3N_4. In brief, according to the FT-IR spectra fully proved the existence of g-C_3N_4, Fe_3O_4 and PPy.

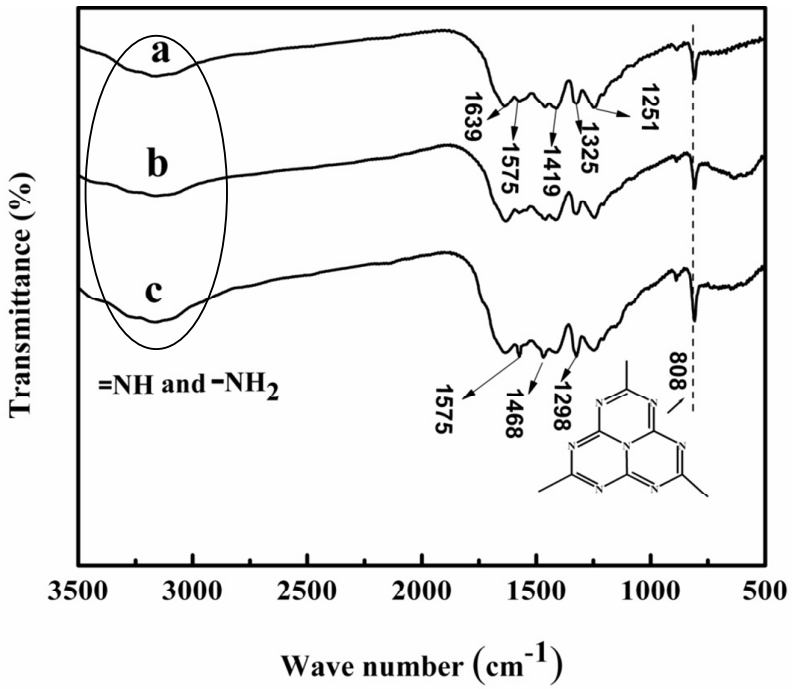

Fig. 2 The FT-IR spectra of g-C_3N_4 (a), Fe_3O_4/g-C_3N_4 (b) and MCIPs (c)

3.1.3 SEM analysis

The SEM spectra of g-C_3N_4, Fe_3O_4/g-C_3N_4 and MCIPs were showed in Fig. 3. It could be seen that the surface of g-C_3N_4 was relatively

smooth, but after coating Fe_3O_4, the surface of g-C_3N_4 became uneven and bulge. Moreover, the materials on the surface of g-C_3N_4 can be seen clearly. Above results indicated that Fe_3O_4 was successfully loaded on the surface of g-C_3N_4. In addition, the image of MCIPs was different with that of Fe_3O_4/g-C_3N_4. The significant change on the surface of MCIPs could be seen obviously by comparison to Fe_3O_4/g-C_3N_4, this must caused by the covered imprinted layer. The EDS images of different samples were also presented in Fig. 3. Compared with Fe_3O_4/g-C_3N_4, the C content of MCIPs increased and the Fe content of MCIPs decreased, which was due to the introduction of surface imprinted layer. In addition, compared with the BET surface areas of the pure g-C_3N_4 and MCIPs showed in Fig. S1, the BET surface area of the pristine g-C_3N_4 was about 5.8 $m^2\ g^{-1}$. After PPy was coated, the BET surface area of MCIPs increased to 20.2 $m^2\ g^{-1}$, the changed of BET surface area might be related to a large number of Fe_3O_4 nanoparticles and imprinted cavities. Moreover, the increased BET surface area was consistent with results of SEM, and proved that the perfection of imprinting once again.

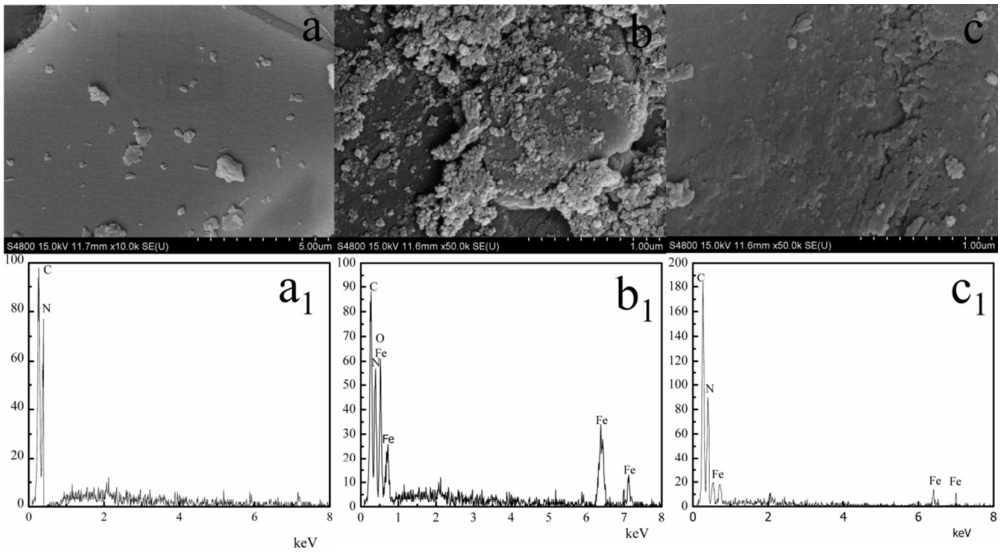

Fig. 3SEM and EDS images of g-C_3N_4 (a, a_1), Fe_3O_4/g-C_3N_4 (b, b_1) and MCIPs (c, c_1)

3.1.4 TEM analysis

Fig. 4 showed the typical TEM images of pure g-C_3N_4, Fe_3O_4/g-C_3N_4, and MCIPs, and high-resolution TEM (HRTEM) of Fe_3O_4/g-C_3N_4. It can be seen that the big sheet structure of g-C_3N_4 was covered by small particles of Fe_3O_4, whereas the Fe_3O_4 nanoparticles have sizes ranging from 5 nm to 10 nm and they were not agglomerated (Fig. 4b). Fig. 5(d) showed HRTEM image of Fe_3O_4/g-C_3N_4. It was clear that the lattice plane with spacing of 0.25 nm, confirmed the g-C_3N_4 sheet could serve as a support to bind with Fe_3O_4 nanoparticles. Compared with the image of MCIPs (Fig. 4c), it seemed that a thin layer aggregated on the surface of Fe_3O_4/g-C_3N_4 and the spherical Fe_3O_4 could not be seen clearly, the changed of this two images must caused by the covered PPy. And the result was in accordance with SEM image. Therefore, the TEM image

further evidence that PPy were successfully assembled onto the surface of Fe_3O_4/g-C_3N_4.

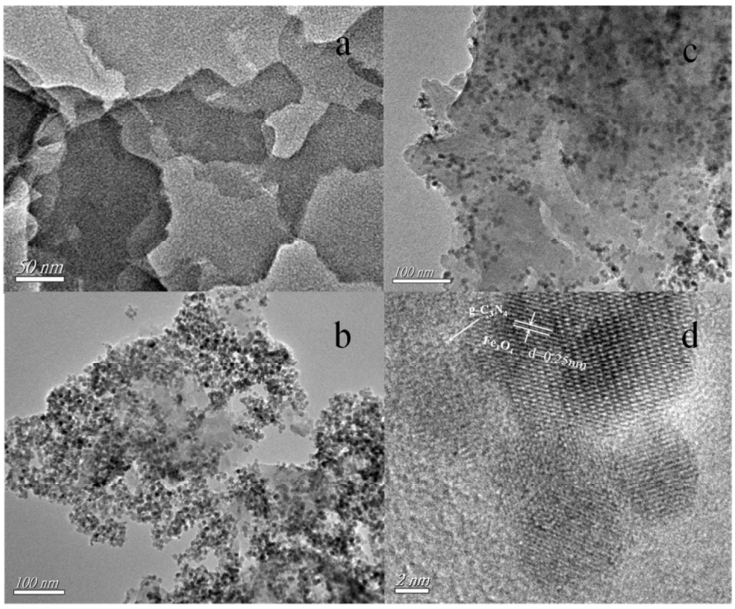

Fig. 4 TEM images of g-C_3N_4 (a), Fe_3O_4/g-C_3N_4 (b) and MCIPs (c), HRTEM of Fe_3O_4/g-C_3N_4 (d)

3.1.5 Elemental analysis

The elemental content of different samples was shown in Table 1.The C/N molar ratio of g-C_3N_4 was 0.734, which was closed to the theoretic value of g-C_3N_4, this result proved that g-C_3N_4 was successfully prepared by calcination melamine [37-39]. In addition, compared with the pure g-C_3N_4 and MCIPs, the content of N, C, and H decreased from 59.82546%, 37.13942% and 2.03588% to 53.97383%, 35.88362% and 1.31395%, respectively, through the calculation, the content of Fe_3O_4 nearly 10%, this was consistent with initial dosage, meaning that Fe_3O_4 was also introduced onto the surface of g-C_3N_4. Furthermore, after the

Fe_3O_4/g-C_3N_4 was modified by imprinting layer, the content of N, C and H were significant increased in MCIPs, this result indicated that the surface of Fe_3O_4/g-C_3N_4 was successfully imprinted.

Table. 1 Results for the elemental composition of different samples by elemental analysis

Samples	N (%)	C (%)	H (%)
g-C_3N_4	59.82546	37.13942	2.03588
Fe_3O_4/g-C_3N_4	53.97383	35.88362	1.31395
MCIPs	55.09838	37.14768	1.92486

3.1.6 TG analysis

The TG curves of g-C_3N_4 and MCIPs were shown in Fig. 5, the g-C_3N_4 was stable from the room temperature to 505°C，however, the weight decreased rapidly in the temperature range from 505°C to 720°C, indicating that the g-C_3N_4 started combustion in the air and almost all of g-C_3N_4 generated gas when the temperature reached 720°C [40]. According to the curve of Fig. 5b, a slight weight loss of MCIPs (5.4%) could be seen from room temperature to 200°C, this might due to the evaporation of water. Furthermore, with the temperature increasing from 200°C to 505°C, the weight loss of MCIPs (5.9%) must attribute to the loss of organic residues from imprinted layer on the surface of Fe_3O_4/g-C_3N_4 [3]. The weight loss between 505°C and 720°C was assigned to the decomposition of the g-C_3N_4. The remaining mass (9.7%)

was attributed to Fe_3O_4, also contained remnants of the small amounts of ashes. Because of melting point of Fe_3O_4 was much higher than the experimental temperature. Throughout the analysis, this completely proved that both MCIPs and g-C_3N_4 have good thermal stability.

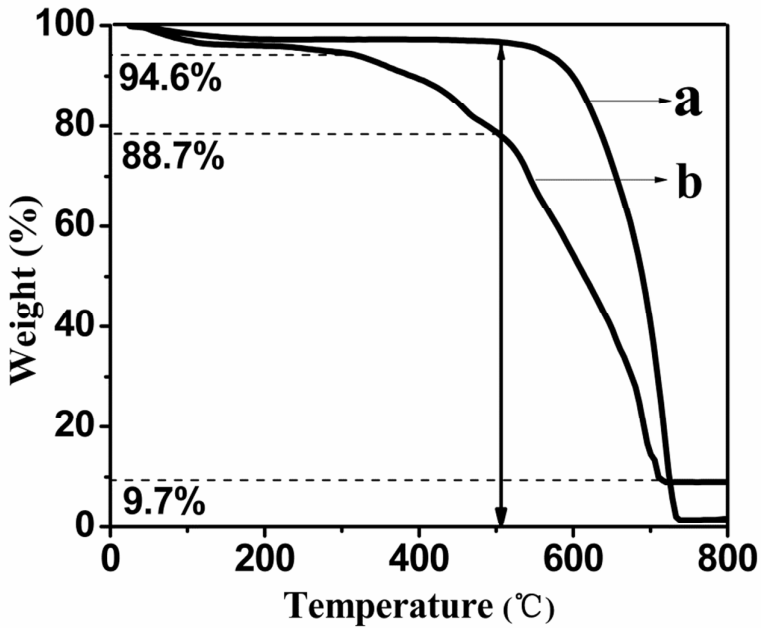

Fig. 5 The thermogravimetric analysis of g-C_3N_4 (a) and MCIPs (b)

3.1.7 VSM analysis

The magnetic property test was measured by vibrating sample magnetometer (VSM) system at room temperature, the magnetic hysteresis loops of the sample Fe_3O_4/g-C_3N_4 and MCIPs were showed in Fig. 6. While the magnetization saturation (Ms) values of Fe_3O_4/g-C_3N_4 and MCIPs were 13.87 emu g^{-1} and 3.64 emu g^{-1}, respectively. This weakening magnetism of MCIPs might be caused by the effect of incremental imprinted layer, the iron oxide in unit weight sample content this could be reduced. However, from the photograph (inset) could be

observed clearly that MCIPs were easily separated by a magnet, indicating that the MCIPs still possessed excellent magnetic separation performance.

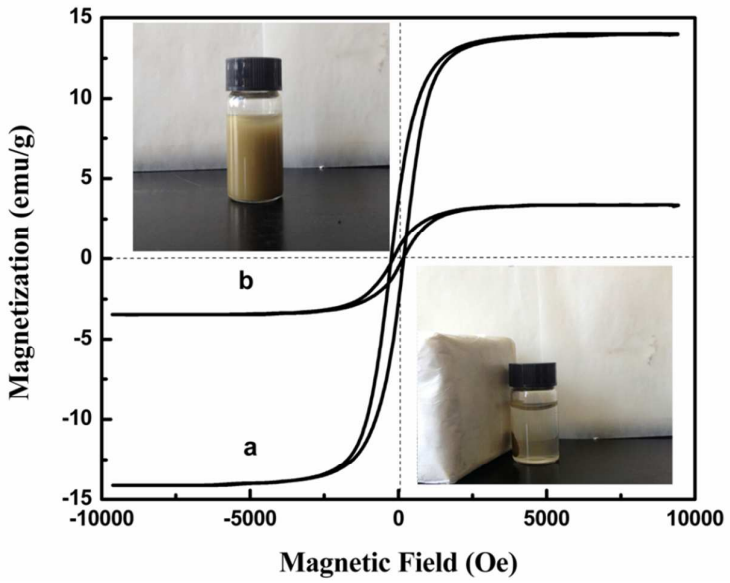

Fig. 6 Hysteresis loops of: Fe_3O_4/g-C_3N_4 (a) and MCIPs (b).Inset image was MCIPs suspension water (left) and MCIPs were attracted by magnetic field (right)

3.1.8 PL analysis

As well known that the PL spectrum originated from the radiative recombination of the free electron-hole pairs and helped clarify the migration and recombination processes of electron-hole pairs in a semiconductor photocatalyst. It could be seen clearly in Fig. 7, the PL intensity of MCIPs decreased significantly compared to pure g-C_3N_4, the weaker intensity of the peak represented the lower recombination rate of photoinduced electron-hole pairs in MCIPs. This could be attributed to the easy transfer of carriers between PPy, Fe_3O_4 and g-C_3N_4. Due to the high conductivity of PPy and Fe_3O_4 as well as the synergistic effect of

PPy, Fe_3O_4 and g-C_3N_4, reduced the recombination rate of electron-hole pairs. Although the PL intensity of the MCIPs was slightly higher than MCNIPs, nevertheless, MCIPs has higher activity for MBT, this also indicating the imprinted cavities and recognition capability took an essential role in enhancing photocatalytic performance and selective photodegradation.

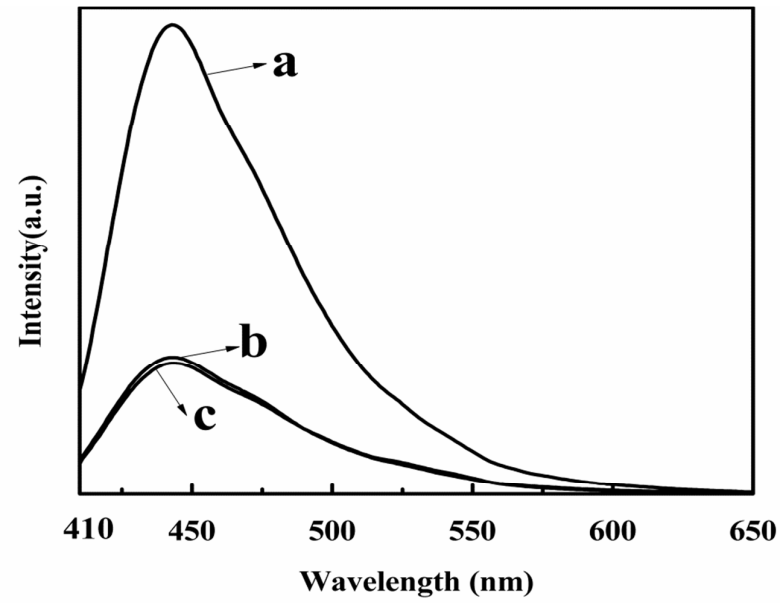

Fig. 7 PL spectra of pure g-C_3N_4 (a), MCIPs (b) and MCNIPs (c)

3.2 Visible-light photocatalytic activity of MCIPs

3.2.1 Adsorption experiments

The adsorption experiments were carried out in accordance with section 2.5. The adsorbing curves of the MCIPs and g-C_3N_4 were showed in Fig. 8. In about 40 min, the solution almost reached adsorption-desorption equilibrium, the adsorption amounts of MCIPs were much greater than g–C_3N_4. The difference adsorption ability could

be attributed to the reason of large numbers of imprinting cavities in the imprinted polymers surface, the increased BET surface area enhanced adsorption ability. Another important reason，as the cavities consistent with the target structure, leading to MCIPs contain high recognition and adsorption more target pollutant.

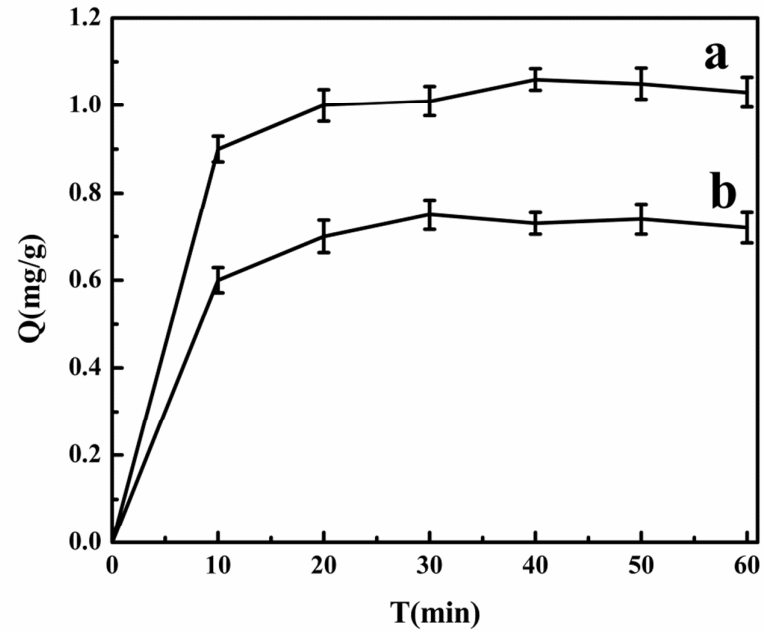

Fig. 8 Adsorbing results of MCIPs (a) and g-C_3N_4 (b) on MBT

3.2.2 The investigation of different polymerization time

Fig. 9 presented the time course of MBT concentrations during the photocatalytic progress. As polymerization time was a very important consideration, in this case, a series of polymerization times were used to synthesis different imprinted photocatalysts. The different polymerization times also revealed the catalytic effect, with the appropriate polymerization time, PPy was well embedded in the surface imprinted layer, as a result of the effect of polymerization time were rather

complicated, if the time was shorter, pyrrole could not polymerize well. On the contrary, the long polymerization time might increase the bonding degree of polymer, and the strong bonding obstacle the removal of template molecules. Therefore, the following experiments, 24h was chosen as the optimum polymerization time to prepare MCIPs. More importantly, the different polymerization time will influence the degree of polymerization for PPy. However, the different degree of polymerization will affect HOMO and LUMO levels of PPy. Therefore, must find the appropriate HOMO and LUMO levels of PPy and match the band gap of g-C_3N_4, to achieve a synergistic catalytic effect, so we proved by experiments, which 24 h was the most suitable time of polymerization [41]

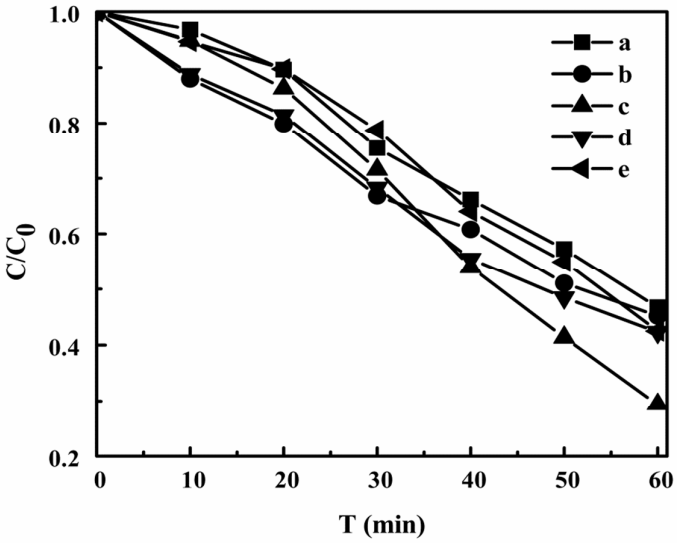

Fig. 9 Effect of polymerization time on degradation of MBT

(a) 6h, (b) 12h, (c) 24h, (d) 36h, (e) 48h

3.2.3 The investigation of different amount of pyrrole

The dosage of pyrrole was another importance role in synthesis of imprinted photocatalysts. As displayed in Fig. 9. The photocatalyst exhibite highest photocatalytic activity when the dosage of pyrrole was 6 mmol. On the one hand, with so less dosage of pyrrole, that PPy could not be polymerized on the surface of Fe_3O_4/g-C_3N_4 incompletely and resulting weaken transmitting ability for photogenerated electrons. Meanwhile the imprinted cavities would also decreased and reduced the recognize ability to MBT, further result lower photocatalytic activity. On the other hand, as the amount of PPy increased, the imprinted layer became thicker, since the superfluous PPy was generated, the thicker imprinted layer will affect the absorption of light, limited for charge transfer and parts of the g-C_3N_4 semiconductor surface could not be excited under visible light irradiation, thereby leading to lower photocatalytic efficiency. Consequently, in the following experiment, the adding dose of pyrrole was 6 mmol.

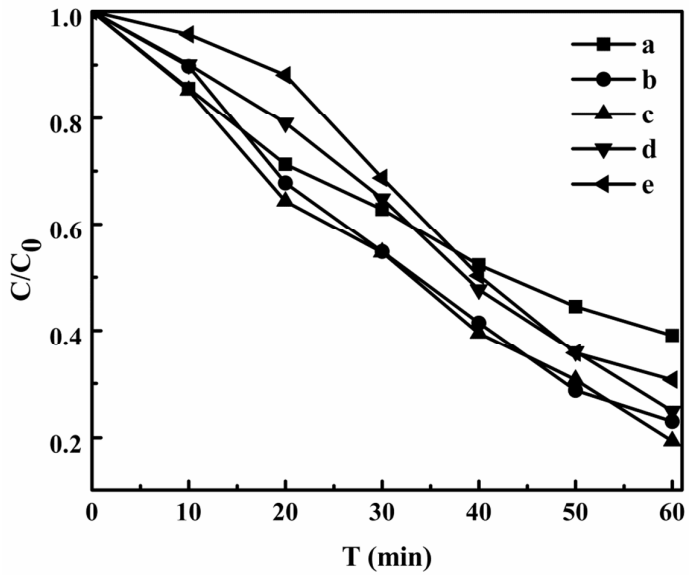

Fig. 10 Effect of the adding dose of pyrrole on degradation of MBT

(a) 0.075mmol, (b) 3mmol, (c) 6mmol, (d) 7.5mmol, (e) 9mmol

3.2.4 Selectivity experiment

The purpose of the present work was selectivity recognition for template molecule. In order to test the advantage of MCIPs, the NMCIPs and pure g-C_3N_4 for degradation experiments were prepared under the same conditions. Fig. 11 (A) showed the photocatalytic effect of MCIPs, MCNIPs and g-C_3N_4 on degradation of MBT for 60 min under the visible light. Furthermore, we discussed why the degradation effect of MCIPs was the highest and g-C_3N_4 was the lowest. For g-C_3N_4, the lowest degradation must be caused by lack of conductive imprinting layer, no surface imprinted cavities, and then loses the recognition capability to MBT, while the degradation of the MBT was correspondingly decreased. However, despite the fact that the MCNIPs had conductive imprinting

layer, there were no imprinted cavities, result to the degradation effect lower than MCIPs. The MCIPs bought out excellent activity toward the template pollutants in this work, which was attributed to the conductive imprinting layer and surface imprinting cavities forming by template molecules, this fully demonstrated the superiority of MCIPs.

In order to further highlight the advantage of selectivity, another experiment on degradation of danofloxacin mesylate was made, the concentration curves were showed in Fig. 11 (B), the catalyst of g-C_3N_4, MCIPs and MNCIPs was as same as above, the photodegradation effect of MCIPs on degradation danofloxacin mesylate, was decreased rapidly. That was due to the different structures of danofloxacin mesylate, which larger than the imprinted molecule, the absence of binding sites, leading to lower selectivity. It was obvious that, the photodegradation effect of MCIPs and MCNIPs was similar and higher than pure g-C_3N_4 on degradation of danofloxacin mesylate, this also showed that the conductive imprinted layer played a critical role, which was also promote the transmission and separation of electrons and holes. Thus further demonstrated that the importance of the imprinting cavities on target pollutants degradation.

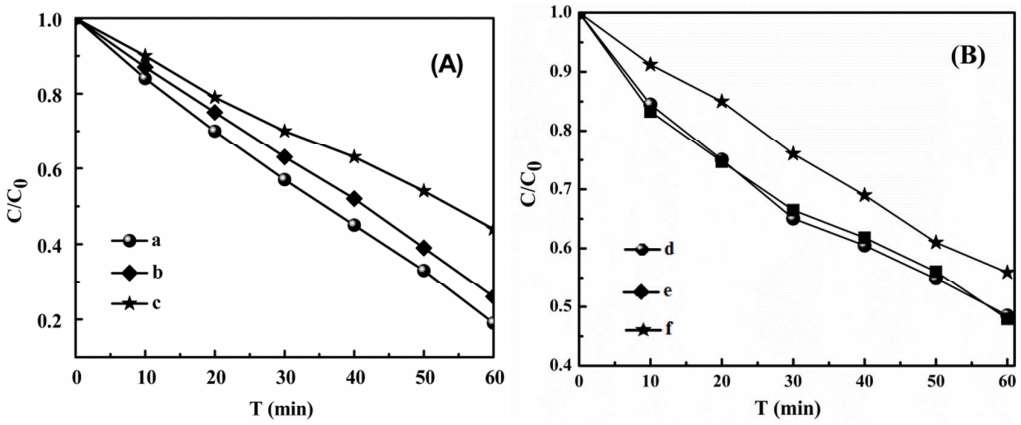

Fig. 11The effect of degradation of MBT (A) and danofloxacin mesylate (B) with MCIPs (a, d), MCNIPs (b, e), g-C_3N_4 (c, f),

3.2.5 Photocatalytic stability

For MCIPs, besides the photocatalytic activity and selectivity were demanded, the photocatalytic stability was crucially important for practical applications. The recycling capability of the MCIPs was verified by carrying out a five-run test of photocatalytic degradation MBT. Fig. 12 revealed that degradation rate was no obvious decreased after the five-run test, which indicating that MCIPs had excellent photocatalytic stability.

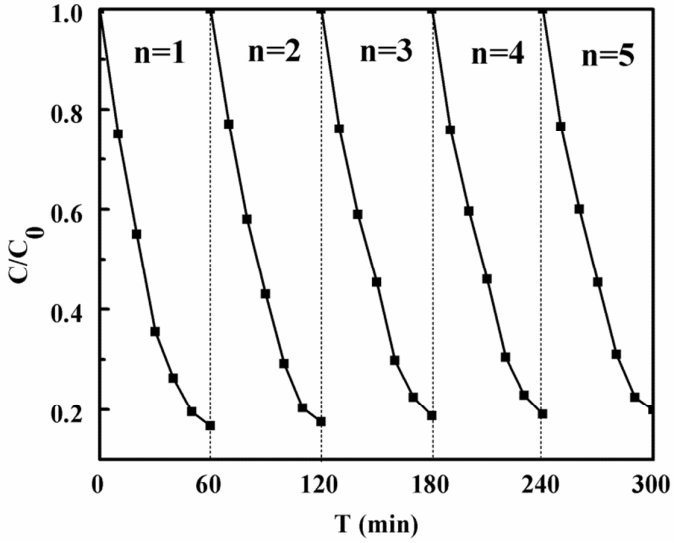

Fig. 12 Recyclability of MCIPs on degradation of MBT under visible-light irradiation

3.3. Photocatalytic mechanism

3.3.1 Active species trapping and $\cdot O_2^-$, h^+ and ·OH quantification experiments

It was generally known that the $\cdot O_2^-$, h^+ and ·OH were the major reactive species for photodegradation. For detecting the active species of MCIPs during photocatalytic reactivity, 1 mmol triethanolamine (OA a quencher of h^+), 1 mmol isopropanol (IPA a quencher of ·OH), and 1 mmol benzoquinone (BQ a quencher of $\cdot O_2^-$) [42-46] were added into reaction solution during the degradation experiment, respectively. The detection process was as same as the experimental photodegradation process. The results were shown in Fig. 13. The degradation efficiency of MBT was 85% when no scavenger was added. However, when adding OA into the solution, the photodegradation rate of MBT decreased to 5%, revealing that the photogenerated holes played such a central role for degradation. When adding IPA into the reactions, the degradation rate of MBT was hardly decreased, indicating that ·OH were not the main active species for degradation. Also, the effect of $\cdot O_2^-$ could not negligible, as could be seen from the graph which adding BQ, also inhibited nearly half of degradation rate. Therefore, the influence degree was $h^+ > \cdot O_2^- > \cdot OH$ for the MCIPs.

The photodegradation rate (η) was calculated by using the following formula: C_0 was the initial concentration and C the concentration of

reaction solution.

$$\eta = (1 - \frac{C}{C_0}) \times 100\% \quad (1)$$

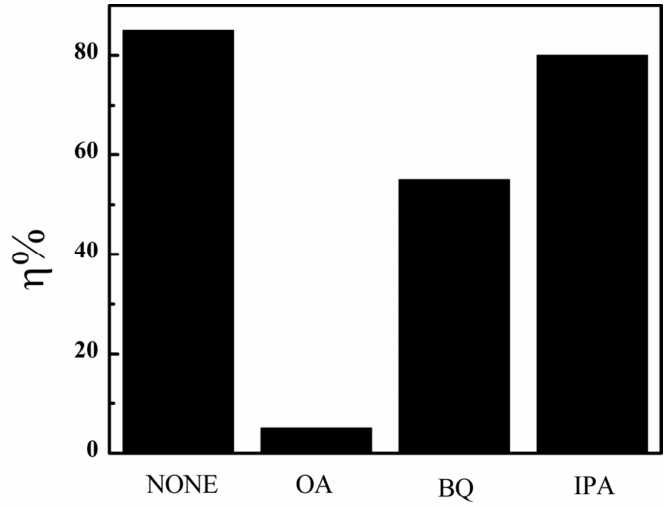

Fig. 13 Effects of a series of scavengers on the photocatalytic efficiency of MCIPs

3.3.2 Photocatalytic mechanisms of the MCIPs

Fig. 14 showed the photocatalytic degradation process of degradation of MBT with MCIPs. When the as-prepared composites were irradiated under visible-light, both g-C_3N_4 and PPy could easily absorb visible light. As PPy was eminent electronic conductor [47], the polymer could absorb photons and promote an electron from the ground state into an excited state under visible-light irradiation. The lowest unoccupied molecular orbital (LUMO) levels and the highest occupied molecular orbital (HOMO) levels of PPy generate electrons and holes, respectively [26, 48]. Meanwhile, electrons ccould be excited to the conduction band and leave holes in the valence band of g-C_3N_4. Afterward, the photogenerated

electrons might injected to the conduction band of inner g-C_3N_4. Furthermore, the leaved holes of g-C_3N_4 were transferred to the surface of thick PPy layer. Therefore, the recombination rate of electron-hole pairs in the composite system was reduced significantly. As there were a large number of O_2 and H_2O adsorbed on the PPy surface, which could react with e^-, then generate $\cdot O_2^-$ and H_2O_2, and react with MBT, as same as the (h^+), then produced CO_2, H_2O and other smaller molecular. The possible photodegradation mechanism and charge transfer processes were displayed as follows:

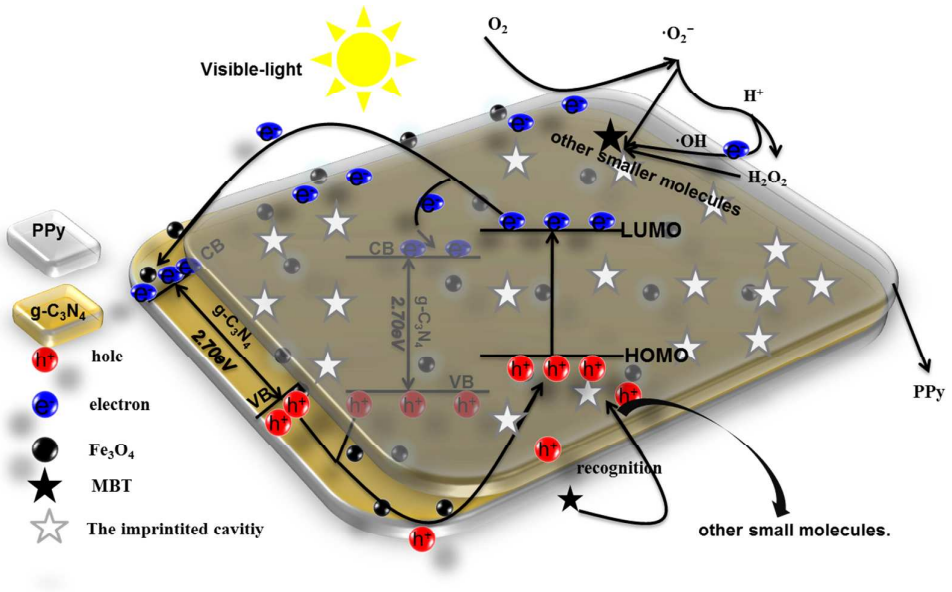

Fig.14 Schematic illustration of degradation of MBT with MCIPs under visible light irradiation.

$$g - C_3N_4 + h\nu \rightarrow g - C_3N_4(h^+ + e^-) \quad (2)$$

$$PPy + h\nu \rightarrow PPy\ (h^+ + e^-) \quad (3)$$

$$PPy(e^-) \rightarrow g - C_3N_4(h^+) \quad (4)$$

$$g - C_3N_4(h^+) \rightarrow PPy(e^-) \quad (5)$$

$$H_2O \rightarrow H^+ + OH^- \quad (6)$$

$$2g - C_3N_4(e^-) + 2H^+ + O_2 \rightarrow H_2O_2 \quad (7)$$

$$H_2O_2 + e^- \rightarrow \cdot OH + OH^- \quad (8)$$

$$g - C_3N_4(e^-) + O_2 \rightarrow \cdot O_2^- \quad (9)$$

$$\cdot O_2^- + 2H^- + 2e^- \rightarrow 2 \cdot OH \quad (10)$$

$$PPy(h^+) + MBT \longrightarrow \text{other small molecules (majority)} \quad (11)$$

$$\cdot O_2^- + MBT \longrightarrow \text{other small molecules} \quad (12)$$

$$H_20_2 + MBT \longrightarrow \text{other small molecules} \quad (13)$$

$$\cdot OH + MBT \rightarrow \text{other small molecules} \quad (14)$$

3.3.3 MS analysis

Mass spectrometry (MS) was widely used to discuss the possible mechanism of photodegradation. As shown in Fig. S2 (in the supporting information), could be found that as time went on, the characteristic peak of MBT (m/z = 168) had became smaller and smaller. This illustrated that MBT had been decomposed into other intermediate degradation products then these substances were gradually decomposed to CO_2, H_2O and other smaller molecular. According to MS, the mechanism was speculated as follows:

In the MS, the peak of (m/z=168, m/z=139, m/z=108, m/z=125) were analyzed in the processes of photodegradation. Firstly, the target were attracted by active substance and lost group of –SH, was generated (A).

The formation of (B) might due to the fact that (A) was quickly binding with H in the solution, that was why the peak of m/z=168 became smaller. As N=C was not stable, and broke the N-C double bond of (B).Thereby, (C) was generated easily under the irradiation of light. Subsequently, the group of -S-CH_3 in (C) might fracture, and formation of ·CH_3 and ·SH, then the two group occurrence of rearrangement, along with the reaction, a small amount of (D) and (E) might generate. Finally, the (C), (D) and (E) were further degradation to CO_2, H_2O and other small molecules.

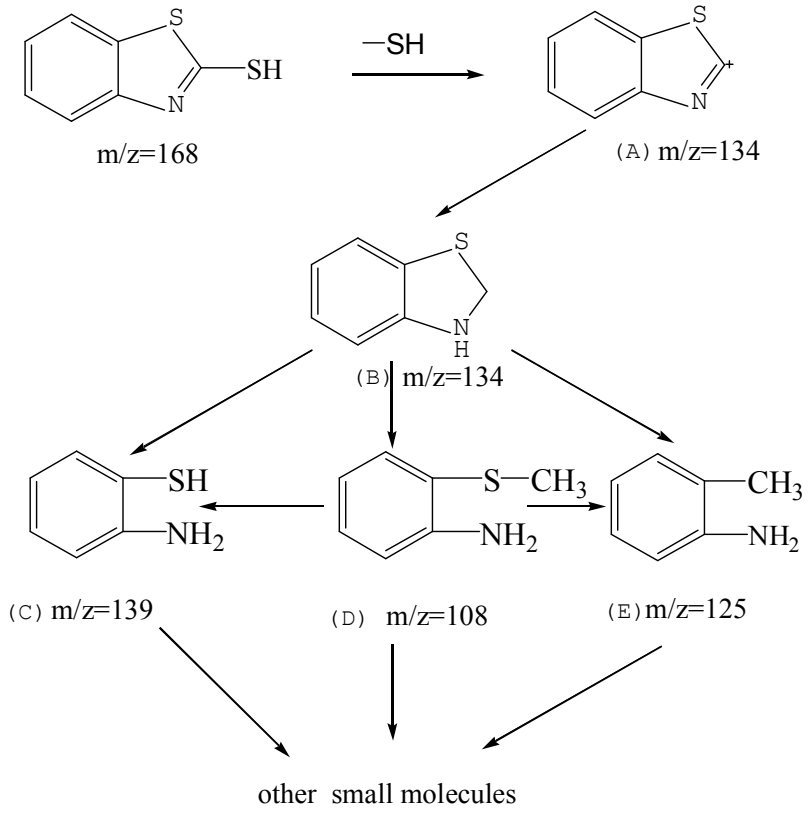

Fig. 15 The photodegradation mechanism of MBT over MCIPs

4. CONCLUSIONS

In summary, a novel with ease preparation method, coupled with the low cost and stability magnetic conductive imprinted g-C_3N_4 has been fabricated successfully in suspension polymerization. For the imprinted catalyst, through a series investigation of factors, showed the optimized photocatalytic activity and high adsorption capacity for the target pollutants as well as outstanding recognizing behavior toward MBT when the polymerization time was 24 h and the adding dose of pyrrole was 6 mmol. And the photodegradation rate for MBT with MCIPs reached nearly 85% in 60 min under the visible light irradiation, the degradation rate of MCIPs improved nearly 40% than pure g-C_3N_4. More importantly, the intermediate products were analyzed by MS while proving that there was no harmful substance generated in the degradative process. Moreover, the PL improved separation of photogenerated electron−hole pairs and higher efficiency of cavity recognition.

ACKNOWLEDGMENTS

We gratefully acknowledge the natural science foundation of China (No. 21306068 and 21407059), the natural science foundation of jiangsu province (Nos. BK20130477, BK20130480, BK20130487 and BK20140532), the financial support of china postdoctoral science foundation (No. 2014T70486 and 2011M500863) and the innovation programs foundation of jiangsu province (Nos. CXZZ13_0693)

Supporting Information

Nitrogen sorption isotherms of g-C_3N_4 (a) and MCIPs (b) calculated from desorption branch by BJH method, Mass spectra of 2-Mercaptobenzothiazole in photodegradation process used MCIPs.

AUTHOR INFORMATION

Corresponding author

*Tel.: +86 511 8879 0187 Fax. : +86 511 8879 1800

E-mail address: gchxz206@126.com

Notes

The authors declare no competing financial interest.

REFERENCES

1. Yan, S. C; Lv, S. B.;Li, Z. S; Zou, Z. G. Organic–inorganic composite photocatalyst of g-C_3N_4 and TaON with improved visible light photocatalytic activities. Dalton Trans. **2010**, 39, 1488–1491.

2.Chong, M. N.; Jin, B. Photocatalytic treatment of high concentration carbamazepine in synthetic hospital wastewater. J. Hazard. Mater. **2012**, 199, 135-142.

3. Luo, Y.Y.; Lu, Z. Y.; Jiang, Y. H.; Wang, D. D.; Yang, L. L.; Huo, P. W.; Da, Z, L.; Bai, X. L.; Xie, X. L.; Yang, P. Y.Selective photodegradation of 1-methylimidazole-2-thiol by the magnetic and dual conductive imprinted photocatalysts based on TiO_2/Fe_3O_4/MWCNTs. Chem. Eng. J. **2014**, 240, 244–252.

4. Shen, X.; Zhu, L. H.; Wang, N.; Zhang, T.; Tang, H. Selective photocatalytic degradation of nitrobenzene facilitated by molecular imprinting with a transition state

analog. Catal. Today. **2014**, 225, 164-170.

5. Lu, Z. Y.; Huo, P. W.; Luo, Y. Y.; Liu, X. L.; Wu, D.; Gao, X.; Li, C. X.; Yan, Y. S. Performance of molecularly imprinted photocatalysts based on fly-ash cenospheres for selective photodegradation of single and ternary antibiotics solution. J. Mol. Catal. A-Chem. **2013**, 378, 91-98.

6.Liu, X. L.; Lv, P.; Yao, G. X.; Ma, C. C.; Huo, P. W.; Yan, Y. S.Microwave-assisted synthesis of selective degradation photocatalyst by surface molecular imprinting method for the degradation of tetracyclineonto Cl-TiO_2. Chem. Eng. J. **2013**, 217, 398–406.

7. Lu, Z. Y.; Zhou, W. C.; Huo, P. W.; Luo, Y. Y.; He, M.; Pan, J. M.; Li, C. X.; Yan, Y. S. Performance of a novel TiO_2 photocatalyst based on the magnetic floating fly-ash cenospheres for the purpose of treating waste by waste. Chem. Eng. J. **2013**, 225, 34-42.

8. Sun, L. M.; Zhao, X.; Jia, C.-J.; Zhou, Y. X.; Cheng, X. F.; Li, P.; Liu, L.; Fan, W. L. Enhanced visible-light photocatalytic activity of g-C_3N_4–$ZnWO_4$ by fabricating a heterojunction: investigation based on experimental and theoretical studies. J. Mater. Chem. **2012**, 22, 23428-23438.

9. Chen, S. F.; Hu, Y. F.; Meng, S. G.; Fu, X. L. Study on the separation mechanisms of photogenerated electrons and holes for composite photocatalysts g-C_3N_4-WO_3, Appl. Catal. B-Environ. **2014**, 564– 573.

10. Xiang, Q. J.; Yu, J. G.; Jaroniec, M. Preparation and enhanced visible-light photocatalytic H_2-production activity of graphene/C_3N_4 composites. The J. Phys.

Chem. C. **2011**, 115, 7355-7363.

11. Dong, G. H.; Zhao, K.; Zhang, L. Z. Carbon self-doping induced high electronic conductivity and photoreactivity of g-C_3N_4. Chem. Commun. **2012**, 48, 6178-6180.

12. Wang, Y. J.; Bai, X. J.; Pan, C. S.; He, J.; Zhu, Y. F. Enhancement of photocatalytic activity of Bi_2WO_6 hybridized with graphite-like C_3N_4. J. Mater. Chem. **2012**, 22, 11568-11573.

13. Liao, G. Z.; Chen, S.; Quan, X.; Yu, H. T.; Zhao, H. M. Graphene oxide modified g-C_3N_4 hybrid with enhanced photocatalytic capability under visible light irradiation. J. Mater. Chem. **2012**, 22, 2721-2726.

14. Zhang, J. S.; Sun, J. H.; Maeda, K.; Domen, K.; Liu, P. Antonietti, M.; Fu, X. Z.; Wang, X. C., Sulfur-mediated synthesis of carbon nitride: band-gap engineering and improved functions for photocatalysis. Energ. Environ. Sci. **2011**, 4, 675-678.

15. Ye, S.; Qiu, L.-G.; Yuan, Y.-P.; Zhu, Y.-J.; Xia, J.; Zhu, J.-F. Facile fabrication of magnetically separable graphitic carbon nitride photocatalysts with enhanced photocatalytic activity under visible light. J. Mater. Chem. A. **2013**, 1, 3008-3015.

16. Lu, Z. Y.; Chen, F.; He, M.; Song, M. S.; Ma, Z. F.; Shi, W.D.; Yan, Y. S.; Lan, J.Z.; Li, F.; Xiao, P. Microwave synthesis of a novel magnetic imprinted TiO_2 photocatalyst with excellent transparency for selective photodegradation of enrofloxacin hydrochloride residues solution. Chem. Eng. J. **2014**, 249, 15–26.

17. Xi, G. C.; Yue, B.; Cao, J.; Ye, J. H. Fe_3O_4/WO_3 Hierarchical Core–Shell Structure: High‐Performance and Recyclable Visible‐Light Photocatalysis. Chem-Eur. J.**2011**, 17, 5145-5154.

18. Kumar, S.; Kumar, B.; Baruah, A.; Shanker, V. Synthesis of Magnetically Separable and Recyclable g-C_3N_4–Fe_3O_4 Hybrid Nanocomposites with Enhanced Photocatalytic Performance under Visible-Light Irradiation. J. Phys. Chem. C. **2013**, 117, 26135-26143.

19. Lu, Z. Y.; Luo, Y.; He, M.; Huo, P. W.; Chen, T. T.; Shi, W. D.; Yan, Y. S.; Pan, J. M.; Ma, Z. F.; Yang, S. Y. Preparation and performance of a novel magnetic conductive imprinted photocatalyst for selective photodegradation of antibiotic solution. RSC. Advances. **2013**, 3, 18373-18382.

20. Ge, L.; Han, C. C.; Liu, J. In situ synthesis and enhanced visible light photocatalytic activities of novel PANI–g-C_3N_4 composite photocatalysts. J. Mater. Chem. **2012**, 22, 11843-11850.

21. Wang, J; Ni, X; Photoresponsive polypyrrole–TiO_2 nanoparticles films fabricated by a novel surface initiated polymerization. Solid State Commun 2008, 146, 239–244

22. Wang, P; Xie, T; Peng, L; Li, H; Wu, T; Water-assisted synthesis of anatase TiO_2 nanocrystals: mechanism and sensing properties to oxygen at room temperature. J Phys. Chem. C. 2008, 112, 6648–6652.

23. Liang, H. C; Li, X.Z; Visible-induced photocatalytic reactivity of polymer-sensitized titania nanotube films, Appl. Catal. B-Environ. 2009, 86, 8–17.

24. Chowdhury, D; Paul, A; Chattopadhyay, A; Photocatalytic polypyrrole–TiO_2-nanoparticles composite thin film generated at the air–water interface. Langmuir. 2005. 21, 4123–4128.

25. Zhang, C. R; Li, Q. L; Li, J.Q; Synthesis and characterization of polypyrrole/TiO_2

composite by in situ polymerization method. Synth. Met. 2008, 160, 1699-1703

26. Zhang, Z. J; Wang, W. Z; Gao, E. Polypyrrole/Bi_2WO_6 composite with high charge separation efficiency and enhanced photocatalytic activity. J. Mater. Sci. **2014**, 49, 7325-7332.

27. Bai,X. J.; Zong, R. L.; Li, C. X.; Liu, D.; Liu,Y. F. Zhu. Y. F. Enhancement of visible photocatalytic activity via Ag@C_3N_4 core–shell plasmonic composite. Appl Catal. B-Environ. 2014,147,82– 91.

28. Li, X. F.; Zhang, J.; Shen, L. H.; Ma, Y. M.; Lei, W. W.; Cui, Q. L.; Zou, G. G. Preparation and characterization of graphitic carbon nitride through pyrolysis of melamine. App. Phys. A. **2009**, 94, 387-392.

29 Zhao, Y. C.; Liu, Z.; Chu, W. G.; Song, L.; Zhang. Z. X.; Yu, D. L.; Tian, Y. J.; Xie, S.; Sun, L. F. Large-Scale Synthesis of Nitrogen-Rich Carbon Nitride Microfibers by Using Graphitic Carbon Nitride as Precursor. Adv. Mater. 2**008**, 20, 1777-1778.

30. Bu, Y.; Chen, Z.; Yu, J.; Li, W. A novel application of g-C_3N_4 thin film in photoelectrochemical anticorrosion. Electrochim. Acta. **2013**, 88, 294-300.

31. Wang, Y. J; Bai, X. J; Pan, C. S; He, J.; Zhu, Y. F. Enhancement of photocatalytic activity of Bi_2WO_6 hybridized with graphite-like C_3N_4. J. Mate. Chem. **2012**, 22, 11568-11573.

32. Jun, Y. S.; Lee, E. Z.; Wang, X. C.; Hong, W. H.; Stucky, G. D.; Thomas, A. From Melamine-Cyanuric Acid Supramolecular Aggregates to Carbon Nitride Hollow Spheres. Adv. Funct. Mater. **2013**, 23, 3661-3667.

33. Li, X. H.; Wang, X. C.; Antonietti, M. Solvent-Free and Metal-Free Oxidation of

Toluene Using O_2 and g-C_3N_4 with Nanopores: Nanostructure Boosts the Catalytic Selectivity. ACS. Catal. **2012**, 2, 2082-2086.

34. Xie, J.; Chen, K.; Lee, H. Y.; Xu, C.; Hsu, A. R.; Peng, S.; Chen, X.; Sun, S. Ultrasmallc (RGDyK)-Coated Fe_3O_4 Nanoparticles and Their Specific Targeting to Integrin rv3-Rich Tumor Cells. J. Am. Chem. Soc. **2008**, 130, 7542-7543.

35. Park, J; An, KJ; Hwang, YS. Ultra-large-scale syntheses of monodisperse nanocrystals. Nat. Mater. **2004**. 3, 891-895.

36. Cheng, Q. L.; Pavlinek, V.; Lengalova, A.; Li, C. Z.; He, Y.; Saha, P., Conducting polypyrrole confined in ordered mesoporous silica SBA-15 channels: preparation and its electrorheology. Micropor, Mesopor. Mat. **2006**, 93, 263-269.

37. Zhang, J. S.; Zhang, M. W.; Yang, C.; Wang, X. C. Nanospherical Carbon Nitride Frameworks with Sharp Edges Accelerating Charge Collection and Separation at a Soft Photocatalytic Interface. Adv. Mater. **2014**, 26, 4121-4126.

38. Wang, X. C.; Maeda, K.; Thomas, A.; Takanabe, K.; Xin, G.; Carlsson, J. M.; Domen, K.; Antonietti, M. A metal-free polymeric photocatalyst for hydrogen production from water under visible light. Nat. Mater. **2008**, 8, 76-80.

39. Zhang, J. S; Guo, F. S.; Wang, X. C. An optimized and general synthetic strategy for fabrication of polymeric carbon nitride nanoarchitectures. Adv. Funct. Mater. **2013**, 23, 3008-3014.

40. Sun, J. X.; Yuan, Y. P.; Qiu, L. G.; Jiang, X.; Xie, A. J.; Shen, Y.H.; Zhu, J.F. Fabrication of composite photocatalyst g-C_3N_4-ZnO and enhancement of photocatalytic activity under visible light. Daltont. T. **2012**, 41, 6756-6763.

41. Ghosh, S.; Kouamé, NA.; Ramos, L.; Remita, S.; Conducting polymer nanostructures for photocatalysis under visible light. Nat, Mater. 2015

42. Cao, J.; Luo, B. D.; Lin, H. L.; Xu, B. Y.; Chen, S.F. Thermodecomposition synthesis of WO_3/H_2WO_4 heterostructures with enhanced visible light photocatalytic properties. Appl. Catal. B-Environ. **2012**, 111, 288-296.

43. Li, W. J.; Li, D. Z.; Lin, Y. M.; Wang, P. X; Chen, W.; Fu, X. Z.; Shao, Y. Evidence for the active species involved in the photodegradation process of methyl orange on TiO_2. J. Phys. Chem. C. **2012**, 116, 3552-3560.

44. Lin, Y. M.; Li, D. Z.; Hu, J. H.; Xiao, G. C.; Wang, J. X.; Li, W. J.; Fu, X. Z. Highly efficient photocatalytic degradation of organic pollutants by PANI-modified TiO_2 composite. J. Phys. Chem. C. **2012**, 116, 5764-5772.

45. Ye, L. Q; Liu, J. Y.; Gong, C. Q.; Tian, L. H.; Peng, T. Y.; Zan, L. Two different roles of metallic Ag on Ag/AgX/BiOX (X=Cl, Br) visible light photocatalysts: surface plasmon resonance and Z-scheme bridge. ACS. Catal. **2012**, 2, 1677-1683.

46. Ye, L. Q.; Gong, C. Q.; Liu, J. Y.; Tian, L. H.; Peng, T. Y.; Deng, K. J.; Zan, L. Bin (Tu)xCl3n: a novel sensitizer and its enhancement of BiOCl nanosheets' photocatalytic activity. J.Mater. Chem. **2012**, 22, 8354-8360.

47. Li, X. C.; Jiang, G. L.; He, G. H.; Zheng, W. J.; Yi Tan, Y.; Wu Xiao, W. Preparation of porous PPy-TiO_2 composites: Improved visible light photoactivity and the mechanism. Chem. Eng. J. **2014**, 236, 480–489.

48. Ullah, H.; Shah, A.-u.-H. A.; Bilal, S.; Ayub, K. Doping and Dedoping Processes of Polypyrrole: DFT Study with Hybrid Functionals. J. Phys. Chem. C. **2014**, 118,

17819-17830.